Publications

Available Online

J. Sci. Res. **15** (1), 1-10 (2023)

JOURNAL OF SCIENTIFIC RESEARCH

www.banglajol.info/index.php/JSR

Electrochemical Activity of Pure and Sn-Doped CeO_2 Nanoparticles using Simple Chemical Precipitation Method

K. Anandalakshmi[1,2*], P. Venkatachalam[1, 2], J. Venugobal[3]

[1]Department of Physics, Periyar Arts College, Cuddalore, Tamil Nadu, India

[2]Department of Physics, Annamalai University, Annamalainagar, Tamil Nadu, India

[3]MRK Institute of Technology, Kattumannarkoil, Cuddalore, Tamilnadu, India

Received 15 October 2021, accepted in final revised form 12 May 2022

Abstract

In the present work, pure and Sn-doped CeO_2 nanoparticles (NPs) were synthesized by the chemical precipitation method calcined at 400 ºC for 4 h. Characterization of NPs was done through X-ray diffraction (XRD), UV-visible, photoluminescence (PL), Fourier transform infrared (FTIR) spectroscopy and high-resolution electron microscope (HRTEM) techniques. The XRD study revealed the crystalline nature, size, and structure of the prepared NPs. The HRTEM results illustrated cubic structure. The UV–visible and PL studies were used to measure the optical behaviors of CeO_2 NPs. The UV-visible showed that the bandgap value of CeO_2 NPs increased from 3.61 to 3.65 eV for different doping concentrations. The XRD study exhibited that the size of the CeO_2 NPs reduced from 11.03 to 7.91 nm. From the TEM analysis, the average size of undoped and 10% Sn-doped CeO_2 NPs was calculated as 9.3 and 7 nm, respectively. A cyclic voltammetric study confirmed that Sn-doped CeO_2 exhibited a higher specific capacitance value than the pure CeO_2. The chemical precipitation method observed excellent redox and oxidation behavior were observed for Sn-CeO_2 NPs by the cyclic voltammetric study. The significant enhancement in the specific capacitance suggested that Sn-doped CeO_2 is a promising material for supercapacitor applications.

Keywords: Sn-doped CeO_2; Chemical precipitation method; Cyclic voltammetric; Supercapacitor.

doi: http://dx.doi.org/10.3329/jsr.v15i1.56206 J. Sci. Res. **15** (1), 1-10 (2023)

1. Introduction

Cerium oxide or ceria (CeO_2) has received considerable interest in researching and developing novel materials due to its wide applications. Cerium oxide has been widely investigated owing to its broad spectrum of scopes such as catalyst, polishing media, and ceramic material for high-temperature devices [1]. Rare earth oxides with different nanostructures are of great importance because of their applications in the high-performance luminescent devices, magnets, biological labeling, and catalysts based on the

* *Corresponding author*: anandhi8888@gmail.com

electronics, optical and chemical characteristics [2,3]. The ceria nanostructures have unique properties of oxygen ion conductivity, high hardness, stability at high temperature, oxygen storage capacity, and reactivity [4]. Ceria can be used in the microelectronics industry's chemical mechanical planarization (CMP) process [5,6]. As an oxygen ion conductivity material, ceria has been used in metal oxide fuel cells [7] and oxygen pumps. The ceria also finds applications in gas sensors [8], sunscreen cosmetics [9], luminescence material [10], etc. The CeO_2 nanoparticles (NPs) were prepared by various chemical and physical methods such as sol-gel [11], hydrothermal [12], sonochemical [13], flame spray pyrolysis [14], homogeneous precipitation [15], co-precipitation [16], reverse micelles process/surfactant-assisted [17] and microwave-assisted heating [18].

Kazazi *et al*. investigated enhanced photocatalytic degradation of methyl orange using Ag/Sn-doped CeO_2 nanocomposite [19]. Yadav *et al*. demonstrated that the smooth spherical morphology of CeO_2 nanoparticles improved surface roughness, membrane porosity, and hydrophobicity for the M-HTI:16 membrane [20]. Kontham *et al*. have reviewed the synthesis of cerium oxide NPs and their biomedical applications such as anti-inflammatory, anticancer, antioxidative, antimicrobial, and antidiabetic [21]. In the present work, ceria nanoparticles were prepared via co-precipitation method. This method has low cost, easy preparation, and industrial viability features. The synthesized CeO_2 NPs were characterized for their optical, structural, and electrical properties in-depth with the X-ray powder diffraction (XRD), transmission electron microscope (TEM), FTIR spectroscopy, UV-visible spectroscopy, and photoluminescence spectroscopy techniques. In this work, the main objectives are

1. to synthesize CeO_2 NPs by co-precipitation method;
2. structural characterization through XRD, TEM, FTIR, UV-visible, and photoluminescence spectroscopy;
3. cyclic voltammetry study to analyze the charge and discharge property. This method could be used in the high-quality application of supercapacitors.

2. Materials and Methods

2.1. *Materials*

The pure and Sn-doped CeO_2 NPs were synthesized using cerium (III) acetate hydrate [$Ce(CH_3CO_2)_3 \cdot xH_2O$], tin chloride dihydrate ($SnCl_2 \cdot 2H_2O$), and oxalic acid dihydrate [$C_2H_2O_4 \cdot 2H_2O$]. All reagents were analytical grade (Sigma-Aldrich Pvt. Ltd, India), and these chemicals were used without further purification. The entire synthesis work was carried out using double distilled water, and ethanol was used for solvent and washing processes.

2.2. *Synthesis of pure and Sn-doped CeO_2* NPs

The pure and Sn-doped CeO_2 NPs were synthesized in an open atmosphere. First, 0.1 M of cerium(III) acetate hydrate [$Ce(CH_3CO_2)_3 \cdot xH_2O$] was dissolved in 50 mL aqueous,

and then Tin chloride dehydrate ($SnCl_2 \cdot 2H_2O$) with various concentrations (2, 4, 6, 8, and 10 wt %) was poured into the above solution. The mixture was stirred magnetically at room temperature until a homogeneous solution was obtained. Then 0.1 M of oxalic acid dihydrate [$C_2H_2O_4 \cdot 2H_2O$] in 50 mL of water was added drop by drop into the above solution. After oxalic acid dihydrate injection, a voluminous yellow precipitate appeared. The precipitate was then purified using the dialysis agent distilled water and ethanol several times to remove impurities. The end product was dried at 80 ºC for 24 h; the powder was calcined at 400 ºC for 4 h to promote crystallization. The pure CeO_2 NPs were also synthesized by following a similar procedure without the doping material.

2.3. *Electrochemical measurement*

Cyclic voltammogram (CV) study was carried out using CH1600C electrochemical analyzer (CH instrument, shanghai, china) with conventional three-electrode cells. They are Ag/AgCl electrode, platinum wire, and glassy carbon electrodes (GCE, 3 nm in diameter) modified by catalysts used as the reference electrode, counter electrode, and working electrode, respectively. After being carefully cleaned, the sample was coated on the surface of the GCE with a load of approximately 4 µg. The cyclic voltametry curves were measured by using an electrolytic solution at room temperature. Investigating the electrochemical affluence of prepared material is one of the important tasks in the energy storage field due to its profitable structural feature and alluring morphological nature.

3. Results and Discussion

3.1. *XRD analysis*

Fig. 1 shows the XRD pattern of pure CeO_2 and Sn-doped CeO_2 NPs. The diffraction peaks observed in the XRD pattern correspond to (111), (200), (220), and (311) planes of CeO_2 NPs. This result indicates all the peaks indexed to pure cubic fluorite structure (JCPDS 34-0394) of CeO_2 with lattice constant a = 5.411 A^o. The pure CeO_2 with various doping concentrations of Sn NPs shows well-defined XRD peaks, indicating the prepared samples' good crystalline nature. No impurity peaks are observed in the diffraction pattern. The average diameter of the CeO_2 nanoparticles was intended using the Scherrer's equation $D = \frac{0.9\lambda}{\beta \cos\theta}$, where β is the full width at half maximum value of maximum intensity peak, θ is the diffraction angle, and λ is the wavelength of X- rays (1.5408A^o) [19]. From Fig. 1, it is observed that the particle size of CeO_2 is abridged after doping with Sn ions. The average crystallite size of pure CeO_2 and Sn-doped CeO_2 are given in Table 1. From Table 1, it can be observed that the crystallite size of CeO_2 was reduced after doping with Sn. Compared with pure CeO_2 and Sn-doped CeO_2 NPs, the crystallite size is decreased from 11.03 to 7.91 nm. This reduction in the crystallite size may be due to the substitute of the cesium atoms by the Sn dopant ions in the crystal lattices. (ionic radius of Sn^{4+} = 0.69A^o as compared to the Ce (ionic radius Ce = 1.098A^o) [22]. On increasing the doping concentration of Sn ions, the lattice parameter values of the cubic

structured CeO_2 are abridged. Arul *et al.* [12] demonstrated that in the Co-doped CeO_2 nanorods, the XRD pattern showed the diffraction peaks corresponding to (111), (200), (220), and (311) planes of CeO_2 - face-centered cubic (fcc) fluorite structure. They observed that the Co-doped CeO2 particle size decreased from 15 nm to 5 nm compared to the pure CeO_2 [22].

Table 1. Particle size, bandgap, absorption, and emission wavelength of pure and Sn-doped CeO_2 NPs.

SL. No.	Doping concentration (wt %)	Particle size (nm)	Band gap (eV)	Absorption wavelength (nm)	Emission wavelength (nm)
1.	Pure CeO_2	11.03	3.61	328	646
2.	CeO_2: Sn (2 wt %)	10.77	3.40	338	645
3.	CeO_2: Sn (4 wt %)	10.09	3.58	357	646
4.	CeO_2: Sn (6 wt %)	9.67	3.60	365	645
5.	CeO_2: Sn (8 wt %)	8.50	3.65	341	646
6.	CeO_2: Sn (10 wt %)	7.91	3.50	341	646

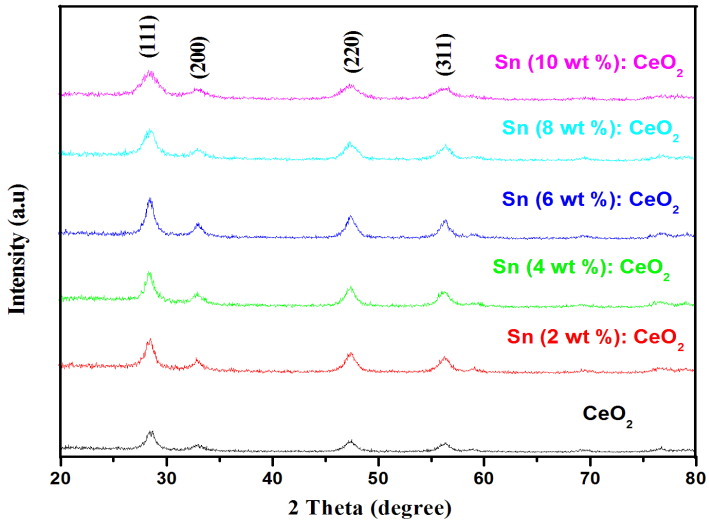

Fig. 1. XRD spectra of undoped and different concentrations of Sn-doped CeO_2 NPs.

3.2. *UV-Visible and photoluminescence analysis*

The UV-visible spectra of the pure and Sn-doped CeO_2 are shown in Fig. 2. The UV-visible absorption peaks of the pure, 2 % Sn-doped, 4 % Sn-doped, 6 % Sn-doped, 8 % Sn-doped, and 10 % Sn-doped CeO_2 particles are found at 343, 364, 346, 344, 339, and 354 nm, respectively. The absorption peaks appeared below 400 nm in the spectra is due to the charge transfer from O 2p to Ce 4f states in CeO_2 [23]. In this study, the above peaks are shifted towards the shorter wavelength side, indicating the decrease in particle size confirmed by the XRD pattern. This increase in energy (blue

shift) and shift towards shorter wavelength are concealed by the existing presence of Ce^{4+} oxygen charge transfer occurring at low coordination Ce^{4+} ions [24]. The optical band gap (E_g) of CeO_2 NPs was found by the following equation $E_g = 1240/\lambda$. The bandgap value of pure CeO_2 is determined as 3.61 eV, and this value is increased up to 3.65 eV for various doping concentrations of Sn [25]. The bandgap of the nanoscale materials is mainly committed to two factors; the quantum size and interface effects. Generally, the quantum size effect leads to a blue shift that predicts an increase in the bandgap value with decreasing particle size, while the interface effect persuades a redshift [23]. Hence, the UV-visible absorption edge is shifted to the lower wavelength side, and a decrease in particle size is likely to be manifested by a blue shift of the absorption edge [26]. Chen and Chang reported the band gap values ranging from 3.56 eV to 3.71eV for CeO_2 NPs synthesized at different calcination temperatures. This increasing band gap value is due to the quantum confinement effect of CeO_2 NPs [27].

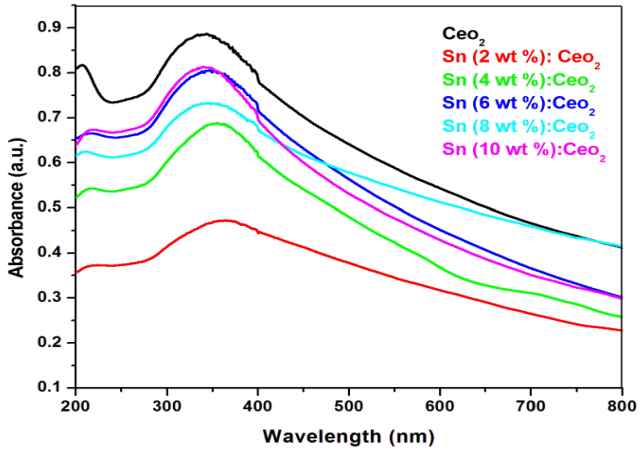

Fig. 2. UV-Vis absorption spectra of undoped and different concentrations of Sn-doped CeO_2 nanoparticles

Photoluminescence (PL) spectroscopy is a powerful technique to investigate the electronic structures of materials. The PL spectra of the pure and Sn-doped CeO_2 were recorded with an excitation wavelength of 350 nm and displayed in Fig. 3. In this work, the PL spectra show the intensity decreases with the increase of the doping concentration. But, at higher concentrations (10 %), the intensity decreases due to the consequence of energy quenching. This indicates the defecting due to Sn doping. The PL emission at 600-700 nm is related to the charge transfer from the Ce 4f level to the O 2p level (valance band). The emission peaks of the Sn-doped CeO_2 samples are found to the red emission. The defect states are between the Ce 4f and O 2p levels, leading to a red emission [18]. This indicated that the defects arose from Sn-doping. Ranjith *et al*. have studied that the PL emission at 469 nm showed bluish green. They have assigned Co doping with CeO_2 increased to 6 % of PL intensity; it might take the Ce 4f states and increase the surface defect states leading to an increased redshift of the CeO_2 nanoparticles by suppressing the Ce-4f to O2p energy transmit level emission [28].

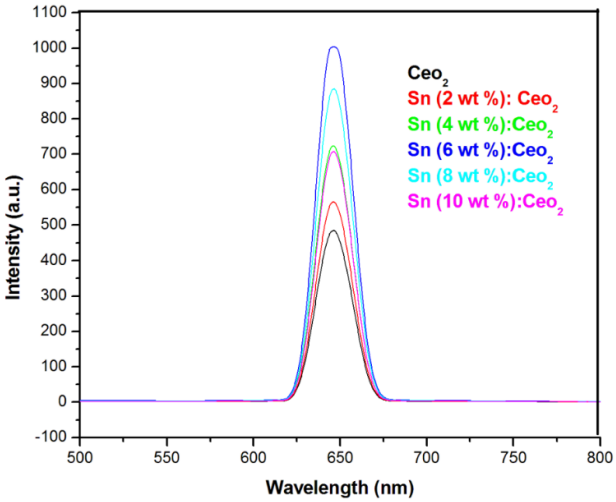

Fig. 3. PL spectra of undoped and different concentrations of Sn-doped NPs.

3.3. *FT-IR analysis*

The FT-IR spectra of the pure and Sn-doped CeO_2 samples are presented in Fig. 4 in the wavelength range from 4000 to 400 cm^{-1}. The strong absorption band at 3404 and 3853 cm-1 is associated with the O-H stretching vibration of residual water and hydroxyl groups. The absorption peak at 1626 cm^{-1} is due to the scissor bending mode of associated water. The peak obtained at 722 and 852 cm^{-1} corresponds to the (Ce-O-O) stretching mode of vibration. However, the bands below 700 cm^{-1} (400-650 cm^{-1}) correspond to the stretching frequency of Ce-O [29]. Earlier report concealed that the FTIR peaks assigned at 1515, 1265, 1130, 1064, 952, 862 cm^{-1} are due to CeO_2 nanoparticles [30]. The assignments of the peaks in the FT-IR spectra of the samples have been given in the reported literature [31,32].

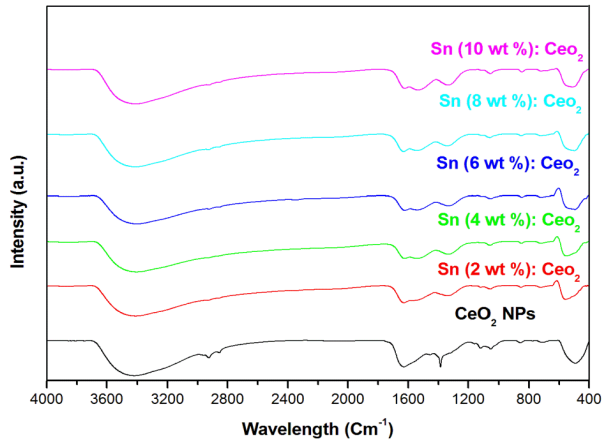

Fig. 4. FTIR spectra of undoped and different concentrations of Sn-doped CeO_2 NPs.

3.4. *TEM analysis*

The morphology of the prepared pure ceria and Sn-CeO_2 NPs samples were analyzed by the TEM and presented in Fig. 5. Fig. 5 shows the corresponding high-resolution TEM images of pure (Figs. 5 a, b, and c) and 10 % Sn-doped CeO_2 NPs (Figs. 5d, e, and f). From the TEM images (Figs. 5a, b, and c), the pure CeO_2 has uniformly distributed cubic shape NPs. The TEM image of the 10 wt% Sn-doped CeO_2 NPs (Fig. 5d, e, and f) has uniform and organized NPs. The average size of undoped and 10% Sn-doped CeO_2 NPs are deliberate 9.3 and 7 nm, respectively, which are in good agreement with the sizes calculated from the XRD technique. These are in accordance with the XRD particle size measurement by using Scherrer's equation. Ranjith *et al*. have observed that the TEM image of the Co-doped CeO_2 NPs was the size of 6-12 nm [28].

3.5. *Electrochemical measurement*

Fig. 6 shows the cyclic voltammetry of the pure and Sn-doped CeO_2 NPs. To estimate the prepared electrode's capacity, cyclic voltammetry and charge-discharge analysis have been conceded out within the potential range of - 1.5 to 1.5 V. Fig. 6 shows a well-defined redox couple anodic and cathodic peak for the pure and Sn-doped CeO_2 NPs. These results show that the pure and Sn-doped CeO_2 NPs have a different redox reaction than the bare GCE. The CV curves of the Sn-CeO_2 are shown to be asymmetric. The redox peaks of Sn-doped CeO_2 NPs indicated the oxidation of Sn. It is also noted that the CV curves of the Sn-CeO_2 show improved capacitance compared to the pure CeO_2-modified electrodes [30-32]. Manibalan *et al.* [33] reported that the Sn-doped CeO_2/GCE cyclic has an electrocatalytic activity for nitrite oxidation. Ibrahim *et al*. demonstrated that the nano-Sn-CeO_2 incorporated GCPE had significant enhancement peak current of DTIC due to the excellent characteristics of nano-Sn-CeO_2 such as high chemical stability and high surface area, good electrical conductivity, etc. [34]. The results accessible in this work show that the Sn-doped CeO_2 NPs prepared by a facile chemical precipitation method could be a high-quality applicant for supercapacitor applications.

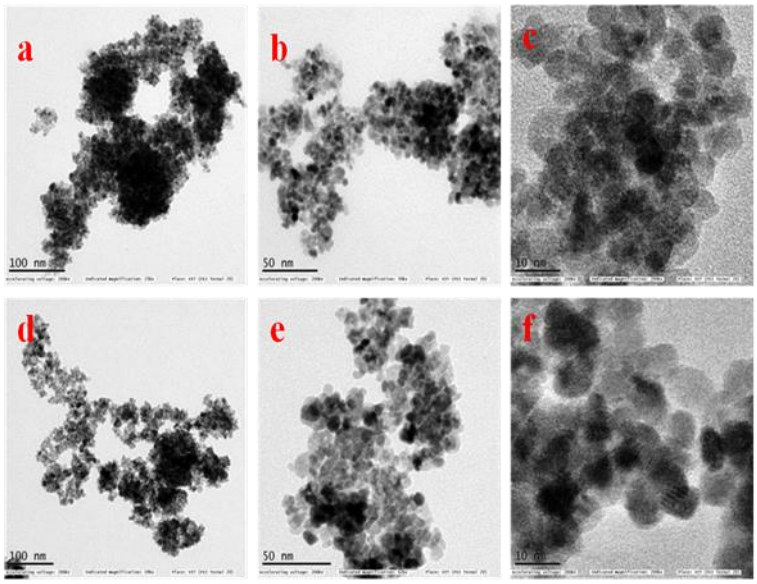

Fig. 5. TEM image of undoped and Sn (10 wt %) doped CeO_2 NPs.

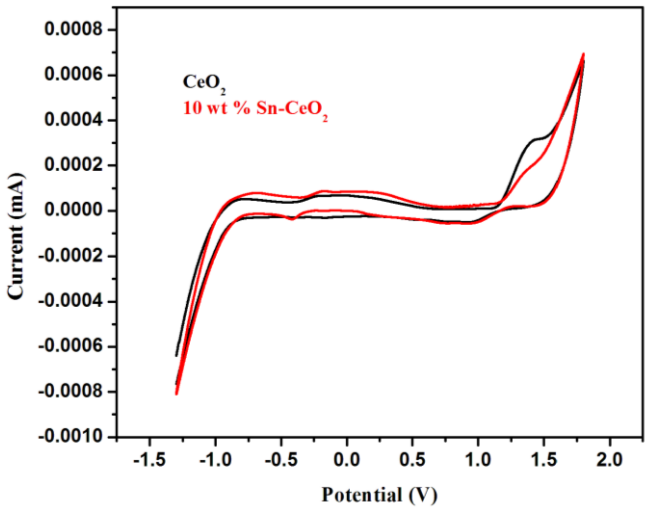

Fig. 6. CV curves for undoped CeO_2 and 10 % Sn-doped CeO_2.

4. Conclusion

The Sn-doped cerium oxide NPs are effectively synthesized using a simple chemical precipitation method. From the XRD analysis, it is found that the obtained NPs were in a cubic structure. The XRD pattern exposed the crystalline nature of the pure CeO_2 and Sn-doped CeO_2, with an average size of the particles was 7.91 nm. The HRTEM images of the samples confirmed the formation of cubic structure nanoparticles. This work reveals

the induced oxygen vacancies related to Sn^{4+} doped CeO_2 NPs, which is electrochemical activity. The calculated band gap energy values of pure and 10 wt % Sn-doped CeO_2 NPs are 3.61 and 3.50 eV from the UV optical spectrum. The Ce–O chemical bonding nature and the presence of functional groups were confirmed from the FTIR spectrum. Finally, the Sn-doped CeO_2 NPs showed excellent supercapacitor performance for energy storage applications. The Sn-doped CeO_2 NPs can be used for real applications for supercapacitors. The cyclic voltammetric study observed excellent redox and oxidation behavior for Sn-CeO_2 NPs by the chemical precipitation method.

References

1. G. Wu, L. Zhang, B. Cheng, T. Xie, and X. Yuan. J. Am. Chem. Soc. **126**, 5976 (2004). https://doi.org/10.1021/cm9605577
2. T. Yu, J. Joo, Y. I. Park, and T. Hyeon, Angewandte Chemie Int. Ed. **44**, 7411 (2005). https://doi.org/10.1002/anie.200500992
3. Z. Wang, Z. Quan, and J. Lin, Inorg. Chem. **46**, 5237 (2007). https://doi.org/10.1021/ic0701256
4. S. Maensiri, C. Masingboon, P. Laokul, W. Jareonboon, V. Promarak, L. A. Philip, and S. Seraphin, Crystal Growth Design. **7**, 950 (2007). https://doi.org/10.1021/cg0608864
5. G. Zhang, Z. Shen, M. Liu, C. Guo, P. Sun, Z. Yuan, B. Li, D. Ding, and T. Chen, J. Phys. Chem. B **110**, 25782 (2006). https://doi.org/10.1021/jp0648285
6. S. Lee, Z. Lu, S. V. Babu, and E. Matijevic. J. Mater. Res. **17**, 2744 (2002). https://doi.org/10.1557/JMR.2002.0396
7. S. K. Sahoo, M. Mohapatra, A. K. Singh, and S. Anand, Mater. Manufact. **9**, 982 (2010). https://doi.org/10.1080/10426914.2010.480995
8. N. Izu, W. Shin, N. Murayama, and S. Kanzaki, Sens. Actuators B: Chem. **87**, 95 (2002). https://doi.org/10.1016/S0925-4005(02)00224-1
9. S. Yabe and T. Sato, J. Solid State Chem. **171**, 7 (2003). https://doi.org/10.1016/S0022-4596(02)00139-1
10. Y. Xijuan, X. Pingbo, and S. Qingde, Phys. Chem. Chem. Phys. **23**, 5266 (2001). https://doi.org/10.1039/b105890h
11. C. Laberty-Robert, J. W. Long, E. M. Lucas, K. A. Pettigrew, R. M. Stroud, M. S. Doescher, and R. D. Rolison, Chem. Mater. **18**, 50 (2006). https://doi.org/10.1021/cm051385t
12. L. Yan, R. Yu, J. Chen, and X. Xing, Cryst. Growth Design **8**, 1474 (2008). https://doi.org/10.1021/cg800117v
13. L. Yin, Y. Wang, G. Pang, Y. Koltypin, and A. Gedanken, J. Colloid Interface Sci. **246**, 78 (2002). https://doi.org/10.1006/jcis.2001.8047
14. L. Madler, W. J. Stark, and S. E. Pratsinis, J. Mater. Res. **17**, 1356 (2002). https://doi.org/10.1557/JMR.2002.0202
15. M. Y. Cho, K. C. Roh, S. M. Park, H. J. Choi, and J. W. Lee, Mater. Lett. **64**, 323 (2010). https://doi.org/10.1016/j.matlet.2009.11.004
16. V. Ramasamy and G. Vijayalakshmi, Superlattices Microstruct. **85**, 510 (2015). https://doi.org/10.1016/j.spmi.2015.05.015
17. H. Li, G. Wang, F. Zhang, Y. Cai, Y. Wang, and I. Djerdj, RSC Adv. **2**, 12413 (2012). https://doi.org/10.1039/c2ra21590j
18. E. Kockrick, C. Schrage, A. Grigas, D. Geiger, and S. Kaskel, J. Solid State Chem. **181**, 1614 (2008). https://doi.org/10.1016/j.jssc.2008.04.036
19. M. Kazazi, B. Moradi, and M. D. Chermahini, Mater. Electronics **30**, 6116 (2019). https://doi.org/10.1007/s10854-019-00913-0
20. A. Yadav, J. R. Mandal, A. B. Panda, and V. K. Shahi, Colloids and Surfaces A: Physicochem. Eng. Aspects **633**, ID 127858 (2022). https://doi.org/10.1016/j.colsurfa.2021.127858

21. S. Kontham, K. Mandava, S. Dosa, F. U. Mohd, O. H. Mohammed, and A. U. Mohammad, Inorg. Nanometal Chem. **52**, 1183 (2022). https://doi.org/10.1080/24701556.2021.1963284
22. A. N. Sabari, D. Mangalaraj, P. C. Chen, N. Ponpandian, P. Meena, M. Yoshitake. J. So-Gel Sci Technol. **64**, 515 (2012). https://doi.org/10.1007/s10971-012-2883-7
23. G. R. Li, D. L. Qu, L. Arurault, and Y. X. Tong. J. Phys. Chem. C **113** 1235 (2009). https://doi.org/10.1021/jp804572t
24. H. Zhang, X. He, Z. Zhang, P. Zang, Y. Li, Y. Ma, Y. Kuang, Y. Zhao, and Z. Chai, Environ. Sci. Technol. **45**, 3725 (2011). https://doi.org/10.1021/es103309n
25. M. A. M. Khan, W. Khan, M. Ahamed, and A. N. Alhazaa, Scientific Reports **7**, 12560 (2017). https://doi.org/10.1038/s41598-017-11074-7
26. L. Brus, J. Phys. Chem. **90**, 2555 (1986). https://doi.org/10.1021/j100403a003
27. H. I. Chen and H. Y. Chang, Ceram Int. **31**, 795 (2005). https://doi.org/10.1016/j.ceramint.2004.09.006
28. K. S. Ranjith, P. Saravanan, S. H. Chan, C. Li Dong, C. L. Chen, S. Y.Chen, and K. Asokan, J. Phys. Chem. C **118**, 27039 (2014). https://doi.org/10.1021/jp505175t
29. A. S. Dezfuli, M. R. Ganjali, H. R. Naderi, and P. Norouzi, RSC Adv. **5**, 46050 (2015). https://doi.org/10.1039/C5RA02957K
30. S. Phoka, P. Laokul, E. Swatsitang, V. Promarak, S. Seraphin, and S. Maensiri, Mater. Chem. Phys. **115**, 423 (2009). https://doi.org/10.1016/j.matchemphys.2008.12.031
31. D. S. Zhang, H. X. Fu, L. Y. Shi, C. S. Pan, Q. Li, Y. L. Chu et al. Inorg. Chem. **46**, 2446 (2007). https://doi.org/10.1021/ic061697d
32. K. Nakagawa, Y. Murata, M. Krishida, M. Adachi, M. Hiro, and K. Susa, Mater. Chem. Phys. **104**, 30 (2007). https://doi.org/10.1016/j.matchemphys.2007.02.047
33. G. Manibalan, G. Murugados, S. Hazra, R. Marimuthu, C. Manikandan, and R. J. Ramalingam, Inorg. Chem. Commun. **135**, ID 109096 (2022). https://doi.org/10.1016/j.inoche.2021.109096
34. M. Ibrahim, Y. Temerk, and H. Ibrahim, RSC Adv. **7**, 32357 (2017). https://doi.org/10.1039/C7RA04331G